



Research

Cite this article: Braconnot P, Kageyama M. 2015 Shortwave forcing and feedbacks in Last Glacial Maximum and Mid-Holocene PMIP3 simulations. *Phil. Trans. R. Soc. A* **373**: 20140424. <http://dx.doi.org/10.1098/rsta.2014.0424>

Accepted: 29 June 2015

One contribution of 12 to a discussion meeting issue 'Feedbacks on climate in the Earth system.'

Subject Areas:

climatology

Keywords:

Last Glacial Maximum and Mid-Holocene climates, ice-sheet and insolation forcing, cloud and surface albedo feedbacks

Author for correspondence:

Pascale Braconnot

e-mail: pascale.braconnot@lsce.ipsl.fr

Shortwave forcing and feedbacks in Last Glacial Maximum and Mid-Holocene PMIP3 simulations

Pascale Braconnot and Masa Kageyama

Laboratoire des Sciences du climat et de l'Environnement,
Orme des Merisiers, bât. 712, Gif-sur-Yvette Cedex 91191, France

Simulations of the climates of the Last Glacial Maximum (LGM), 21 000 years ago, and of the Mid-Holocene (MH), 6000 years ago, allow an analysis of climate feedbacks in climate states that are radically different from today. The analyses of cloud and surface albedo feedbacks show that the shortwave cloud feedback is a major driver of differences between model results. Similar behaviours appear when comparing the LGM and MH simulated changes, highlighting the fingerprint of model physics. Even though the different feedbacks show similarities between the different climate periods, the fact that their relative strength differs from one climate to the other prevents a direct comparison of past and future climate sensitivity. The land-surface feedback also shows large disparities among models even though they all produce positive sea-ice and snow feedbacks. Models have very different sensitivities when considering the vegetation feedback. This feedback has a regional pattern that differs significantly between models and depends on their level of complexity and model biases. Analyses of the MH climate in two versions of the IPSL model provide further indication on the possibilities to assess the role of model biases and model physics on simulated climate changes using past climates for which observations can be used to assess the model results.

1. Introduction

The analyses and understanding of climate feedbacks is at the heart of the Paleoclimate Modeling Intercomparison Project (PMIP) since its first phase [1,2]. Past climate conditions offer an out-of-sample test of climate models

used to produce future climate projections [3]. They provide an understanding on the major feedbacks and their relative role in the Earth's climate response to different external forcings [4], and allow an evaluation of the realism of simulated climate changes through rigorous comparisons with past climate reconstructions from different climate archives [5,6]. These evaluations provide indirect evaluation of the credibility of the representation of climate feedbacks in climate models. There is also a growing interest to use this knowledge to provide constraints on climate sensitivity [4,7–10]. These climate sensitivity estimates suggest that in the case of a doubling of the atmospheric CO₂ concentration, an equilibrium climate sensitivity higher than 6°C is very unlikely [4]. However, the direct link between past and future climate sensitivity is still under debate and requires a better understanding of the feedbacks to refine the methodologies to assess it [5,11,12].

The vegetation feedback received large attention in PMIP [13]. Climate reconstructions clearly highlight substantial changes in past land cover that reflect major differences in regional climates (e.g. [14]). The magnitude of the vegetation feedback is, however, small in the current generation of the Earth system models that includes interactive vegetation and a representation of the carbon cycle [15] compared with early estimates using asynchronous coupling between a climate and a biome model [16] or intermediate complexity models [17]. It has been suggested that the vegetation change was not leading but following other important feedbacks such as sea-ice and snow feedbacks that amplify the temperature response in high latitudes [13,18,19] or soil moisture changes that alter the hydrological conditions in the tropics [20]. It can also be affected by systematic model biases arising from the model climatology, from the representation of the coupling between vegetation and soil moisture that leads to excessive continental drying [21], or from uncertainties in the representation of monsoon changes in the tropics [22–24]. Even though the vegetation feedback is small compared with the 10–20 W m⁻² radiative signature of the cloud feedback at the top of the atmosphere (TOA), it accounts for 2–10 W m⁻² in the changes of the TOA heat budget over Eurasia or Africa and reinforces temperature and precipitation changes in the MH IPSL (Institut Pierre Simon Laplace) model simulations [25]. This has not yet been fully quantified and discussed using the PMIP3/CMIP5 palaeoclimate experiments run as part of CMIP5 [26].

The PMIP3/CMIP5 experiments include simulations of the Last Glacial Maximum (LGM), 21 000 years BP and the Mid-Holocene (MH), 6000 years BP. These two key periods are considered as key benchmarking periods for PMIP simulations [2,5]. The LGM is characterized by the presence of high (*ca* 3000 m over North America) ice-sheets in the Northern Hemisphere (NH), associated with a 120 m sea-level drop, lower greenhouse gas concentration (185 ppm for atmospheric CO₂, 350 ppb for CH₄, 200 ppb for N₂O) and small changes in the latitudinal and seasonal distribution of incoming solar radiation at the TOA resulting from the slightly different astronomical parameters of Earth. The MH, on the other hand, is characterized by enhanced seasonality of the insolation forcing in the NH and a reduced one in the Southern Hemisphere (SH), resulting from changes in the Earth's obliquity and precession, with only small changes in greenhouse gases. PMIP simulations have been performed by imposing the corresponding changes in the climate models' boundary conditions (https://pmip3.lsce.ipsl.fr/p3_c5_design/). Depending on the model complexity, vegetation is either prescribed to be the same as in the pre-industrial (PI) control simulation or interactive. This means that either both vegetation types and leaf area index (LAI) are prescribed, or that the vegetation types are prescribed but LAI is interactive and depends on climate and carbon cycle, or that the vegetation is fully interactive, when the model also includes a dynamical vegetation module (table 1).

Here we focus on shortwave (SW) feedbacks resulting from cloud and surface changes, with the aim of characterizing their respective magnitude for the LGM and the MH and highlighting systematic differences between models. This allows us to discuss the SW cloud feedback that has been shown to have the largest spread among models [6] and to document the impact of vegetation on the radiative budget. The analyses are performed using the Taylor *et al.*'s [37] simplified methodology as in [25] and [2]. The concept of climate sensitivity relates the annual mean forcing (Q), defined as the radiative imbalance at TOA, to the global mean temperature

Table 1. Models considered in the analyses. For the time periods, PI, the PI experiment; LM, the millennium experiment; MH, the Mid-Holocene experiment. The ESM complexity column indicates the ocean–atmosphere coupling the model incorporate interactive aerosols (A), interactive atmospheric chemistry (AC), land carbon (LC) or ocean biogeochemistry (OB), as described in Flato *et al.* [6]. We only consider the subset of models for which the radiative fluxes needed to compute the forcing and feedbacks were available in the ESGF database.

model name	time periods	ESM complexity	resolution	references
Bcc-csm1	PI, MH	LC, OB	A: $128 \times 64 \times L26$ 0: $360 \times 232 \times L40$	Xin <i>et al.</i> [27]
CCSM4	PI, LGM, MH	A, LC	A: $288 \times 192 \times L26$ 0: $320 \times 384 \times L60$	Gent <i>et al.</i> [28]
CNRM-CM5	PI, MH	AC	A: $256 \times 128 \times L31$ 0: $362 \times 292 \times L42$	Voldoire <i>et al.</i> [29]
CSIRO-Mk3-6-0	PI, MH	A	A: $192 \times 96 \times L18$ 0: $192 \times 192 \times L31$	Rotstain <i>et al.</i> [30]
CSIRO-Mk3L1-2	PI, MH	ESM	A: $64 \times 56 \times L18$ 0: $128 \times 112 \times L21$	Phipps <i>et al.</i> [31]
GISS-E2-R	PI, LM, MH	A, AC	A: $144 \times 90 \times L40$ 0: $288 \times 180 \times L32$	Schmidt <i>et al.</i> [32]
IPSL-CM5A-LR	PI, LGM, MH	A, LC, OB	A: $96 \times 95 \times L39$ 0: $182 \times 149 \times L31$	Dufresne <i>et al.</i> [33]
MIROC-ESM	PI, LGM, MH	A, LC, OB	A: $128 \times 64 \times L80$ 0: $256 \times 192 \times L44$	Watanabe <i>et al.</i> [34]
MPI-ESM-P	PI, LGM, MH	LC, OB	A: $96 \times 98 \times L47$ 0: $256 \times 220 \times L40$	Jungclaus <i>et al.</i> [35]
MRI-CGCM3	PI, LGM, MH	A	A: $320 \times 160 \times L48$ 0: $364 \times 368 \times L51$	Yukimoto <i>et al.</i> [36]

change (dT) [38] such that

$$Q = -\lambda dT,$$

where λ is the feedback parameter expressed in Watts per square metre per Kelvin. The feedback parameter can be decomposed into the contribution from the different feedbacks that contribute to balance the radiative forcing. This definition is not well suited to discuss the climate response to the changes in MH forcing, as the annual global average of this forcing is very close to zero. Because of this, we first discuss the global annual mean feedback parameters for the LGM to provide a rapid synthesis of the results already discussed in other publications. Then we compare the MH and LGM surface albedo and SW atmospheric scattering by directly considering their radiative impact at TOA, at the interhemispheric scale, considering the mean annual cycle. We multiply this term by the sign of the temperature change, and call it radiative feedback in the discussion. The specific case of the vegetation albedo feedback is illustrated for the African monsoon. In this region, without snow or ice it directly corresponds to the surface albedo radiative feedback. The aim is to document the strength of the vegetation response in the different simulations and to understand how it is affected by model biases. This last question is only addressed using simulations run with two versions of the IPSL model that only differ in the representation of atmospheric convection and clouds and provide different present-day

climatologies and climate sensitivity [33]. These analyses shed light on the questions that need to be addressed to improve the representation of these feedbacks in climate models.

The analysis method and the estimates of the LGM and MH external forcings are first presented in §2, together with the use of this framework to compare surface albedo and SW cloud feedbacks using the so-called ‘climate sensitivity’ approach for the LGM. Section 3 first compares the radiative feedbacks averaged over the NH for the LGM and MH climates and then highlights model differences in West Africa. The relationship between the vegetation feedback and model physics or biases in the model’s modern climatology is discussed in §5 before a rapid discussion (§6).

2. Forcing and feedbacks at the global scale for the LGM

(a) The simplified framework

We use the Taylor *et al.* [37] simplified approach to quantify the forcing and feedbacks in the SW domain. It uses the fact that the variation of the planetary albedo (α) can be decomposed so as to reflect the individual contributions from the surface albedo (α_s), the bulk atmospheric absorption (μ) and the atmospheric scattering (γ):

$$\Delta\alpha = \frac{\partial\alpha}{\partial\alpha_s}\Delta\alpha_s + \frac{\partial\alpha}{\partial\gamma}\Delta\gamma + \frac{\partial\alpha}{\partial\mu}\Delta\mu + e,$$

where e represents the nonlinear contribution of the different parameters and is negligible here, and Δ represents the difference between two climatic periods. The first two terms of the right-hand side of this equation are the ones we focus on. Changes in atmospheric absorption are small for the MH. They are thus not considered in the comparison below even though we diagnosed it. Indeed our objective is to compare model behaviours for the MH and the LGM, which justifies focusing on the surface albedo and the atmospheric scattering, the latter mostly accounting for the changes in clouds.

In a first step, α , α_s , μ and γ are computed using the simulated incoming and outgoing radiative fluxes at the surface and at the TOA. The equivalent atmospheric model is presented in detail in Taylor *et al.* [37]. These parameters are estimated for each climate and each model. Using this framework, it is possible to quantify the effect of a change in α_s or γ on the net SW flux at TAO between two different climates as

$$\text{feedback}(\alpha_s) = -(\alpha|_{\alpha_{s0}+\Delta\alpha} - \alpha_0)\text{SW}_{i0}$$

and

$$\text{feedback}(\gamma) = -(\alpha|_{\gamma_0+\Delta\gamma} - \alpha_0)\text{SW}_{i0},$$

where the subscript 0 stands for the reference climate, SW_{i0} for the corresponding incoming solar radiation at TOA and Δ represent the difference between the analysed period and the reference period. This methodology cannot be applied to the longwave (LW) part of the radiative spectrum, which will not be considered in his study.

Models have different planetary albedos, resulting from differences in surface albedo or cloud cover, so that the incoming solar radiation difference between two climatic periods translates into different net forcings at the TOA across PMIP simulations. Because of this, we estimate the model insolation forcing using the Hewitt & Mitchell [39] definition

$$f = (1 - \alpha_0)\Delta\text{SW}_i,$$

where α_0 is the planetary albedo simulated for the reference simulation and ΔSW_i is the change in incoming solar radiation between the perturbed and the reference simulations at TOA.

A rough estimate of the error bars associated with these simplified diagnoses is performed by comparing the forcing and feedback estimates we obtained when using the PI climate or the LGM climate as a reference. These error bars are provided in table 2, but not on the figures for clarity. We only discuss in the following differences that are large enough to be significant.

Table 2. LGM SW forcings (W m^{-2}), LGM SW feedback parameters ($\text{W m}^{-2} \text{K}^{-1}$) and LGM global temperature change (K) for five PMIP3/CMIP5 simulations for which the required radiative fluxes at the TOA and at the surface are available in the ESGF database. Error bars in parentheses are estimated from a double computation, using either the PI control simulation or the LGM simulation as a reference to test the effect of the individual factors. For comparison with estimates made for a doubling of carbon dioxide in the atmosphere, the last two column reports the average estimate of the SW cloud and albedo feedbacks computed by Vial *et al.* [40].

Last Glacial Maximum: this study		feedback estimate for future climate					
model name	(W m^{-2})	insolation forcing (W m^{-2})	atmospheric scattering feedbacks ($\text{W m}^{-2} \text{K}^{-1}$)	surface albedo feedback ($\text{W m}^{-2} \text{K}^{-1}$)	globule temperature change (K)		
CCSM4	-3.79 (± 0.1)	0.01	0.11 (± 0.03)	0.32 (± 0.02)	-4.91	~ -0.2	~ 0.35
IPSL-CM5A-LR	-4.90 (± 0.1)	0.01	0.62 (± 0.01)	-0.09 (± 0.01)	-4.59	~ -0.85	~ 0.17
MIROC-ESM	-5.20 (± 0.3)	0.13	-0.48 (± 0.1)	0.18 (± 0.01)	-5.00	—	—
MPI-ESM-P	-4.57 (± 0.3)	0.01	-0.40 (± 0.1)	0.09 (± 0.01)	-4.41	~ -0.43	~ 0.27
MRI-CGCM3	-3.62 (± 0.1)	0.01	-0.02 (± 0.01)	0.39 (± 0.05)	-4.68	~ -0.28	~ 0.35

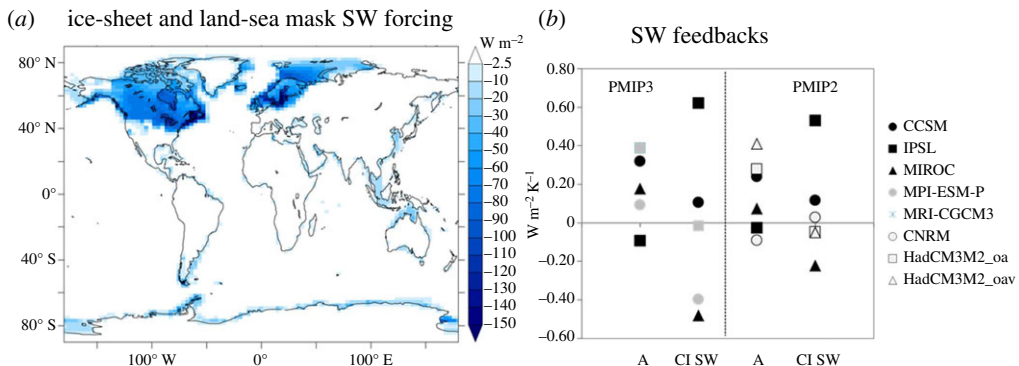


Figure 1. Ensemble mean estimates of the forcings by the ice-sheet and the land mask change from (a) PMIP3 simulations (W m^{-2}) and (b) feedback parameter ($\text{W m}^{-2} \text{K}^{-1}$) from surface albedo (A) and clouds (CI SW) in the SW domain for individual models using PMIP2 and PMIP3 datasets. The subset of models used here corresponds to those for which the requested variables were available on the data archive for the different simulations. The error bars on these estimates is of the order of 0.2 W m^{-2} . (Online version in colour.)

(b) Surface albedo and cloud feedback at the LGM

We first apply this method to diagnose the LGM changes in surface albedo imposed by the presence of the LGM ice-sheet and emerging lands induced by the lower sea-level. Figure 1 presents the model ensemble mean forcing for the PMIP3 simulations (table 1). It can be compared with the similar figure for PMIP2 simulations presented in [2]. This forcing corresponds to the part of the TOA radiative imbalance induced by the change in surface albedo in regions that are affected by the change in ice-sheet and land-sea mask between the LGM and the PI simulations. Over the ice-sheets the negative radiative forcing exceeds 60 W m^{-2} in most places. The difference in the land-sea mask between the LGM and the PI simulation is smaller ($2\text{--}10 \text{ W m}^{-2}$). As discussed in [2] and [25] at the global scale, these two contributions provide larger forcing (ranging from -3.6 to -5.2 W m^{-2} depending on the model, table 2) for PMIP3 than for PMIP2 experiments, because of the difference in ice-sheet reconstructions [41]. As a consequence, PMIP3 LGM simulations are slightly colder than PMIP2 LGM simulations.

The method also allows the comparison of the feedback parameters resulting from surface albedo and from the atmospheric scattering (figure 1). The surface albedo feedback parameter is estimated here from the regions that are not affected by the presence of the ice-sheets or from the change in land-sea mask. It corresponds to model grid boxes with a change in sea-ice, snow or vegetation cover because of plant phenology or vegetation dynamics. The atmospheric scattering is mainly because of changes in cloud (not shown), and we therefore call it the SW cloud feedback parameter in the following. The results plotted in figure 1 are similar to those that are fully discussed in the IPCC AR5 report [42]. For future climate the SW cloud feedback induces a positive feedback in most models (table 2). By contrast, for the LGM, some models produce negative SW cloud feedback, while others have a positive one, suggesting non-symmetrical SW cloud feedbacks between cold and warm periods. The model differences even indicate that the sign of this feedback is uncertain for the LGM. Further investigation is needed to determine which model result is more realistic, based on improved understanding of the processes involved. This figure also highlights that the model spread is larger for the SW cloud feedback parameter than for the surface albedo feedback parameter, as is the case for future climate projections [4,11]. The cloud feedback is therefore a major source of uncertainty whatever the period considered. The ranking of the models is also quite similar for warm and cold climates for the individual feedbacks parameters (within the error bars of individual estimates, table 1). However, there is no systematic and direct ranking between the LGM model results when comparing their respective LGM cooling and the estimates of their climate sensitivity [4]. One of the main reasons is certainly that the relative strength of each feedback is different for those contrasted climates. This should

be related to the fact that the total LGM forcing is a mixture of LW (greenhouse gases) and SW (albedo) forcings that triggers each feedback differently compared with future climate projections that are mainly driven by LW forcing resulting from increase greenhouse gas concentration in the atmosphere. Therefore, despite the ranking for individual feedbacks being similar, the ranking between models is different when considering the sum of all the feedbacks and, thereby, model climate sensitivities. This has strong impacts on our views on the possibility to use regional evaluations of LGM surface temperatures to constrain future climate sensitivity. This might just be a false analogy. New approaches should therefore be based on improved understanding of the feedbacks, in order to find how to best use the regional information from past climate reconstructions to provide efficient constraints on the evaluation of key model processes and thereby on future climate sensitivity.

The comparison of the results obtained for PMIP2 and PMIP3 experiments (figure 1) also shows that the magnitude of the SW feedbacks is larger for PMIP3. Also, the models from the three modelling groups that performed both the PMIP2 and PMIP3 experiments show similar relative ranking between these two phases of PMIP. This suggests that even through the models improved, the representation of land surface and clouds is very similar between the PMIP2 and the PMIP3 versions. The changes were not sufficient to change these models' behaviours. It also suggests that model tuning performed to guarantee equilibrated coupled experiments, generally on each new model version, only marginally alters model feedbacks.

3. Comparison of Northern Hemisphere surface albedo and SW cloud feedback for the LGM and the MH

(a) Northern Hemisphere SW forcings and feedbacks

The MH change in the Earth's astronomical parameters translates into different latitudinal and seasonal variations of insolation, but has only little effect on the annual mean global insolation. The climate sensitivity framework used to discuss the LGM is not appropriate for this climate and would lead to misleading results. The estimates of forcing and radiative feedbacks are nevertheless relevant to understand model responses at seasonal scale. As the MH insolation changes have opposite effects on the two hemispheres, it is also more appropriate to consider hemispheric averages rather than global averages. Here, for simplicity, we only discuss the NH where the seasonality is enhanced during MH, and where the impact of the ice-sheet is larger during LGM. We also consider the radiative feedbacks in Watts per square metre and not the feedback parameters (i.e. feedback divided by the temperature change) to avoid any confusion with the global estimate discussed above for the LGM. The sign of the feedbacks is chosen so that it directly indicates if a feedback is a positive (amplification of the forcing) or a negative (damping of the forcing) feedback.

Figure 2a(i) shows that, as expected from its strong albedo, the LGM ice-sheet and land-sea mask forcing is negative all year long. It reaches its maximum in boreal summer when the incoming solar radiation is at its maximum in the NH. Owing to the large differences in surface albedo, and in the way the LGM land-sea mask has been implemented in the different models, this albedo forcing shows a large model spread which reaches 8 W m^{-2} in June–August. The spread is much smaller for the insolation forcing. Indeed the latter mainly depends on the planetary albedo and all models produce a global mean planetary albedo close to 30% despite large differences in cloud cover. Differences in solar forcing are larger at the regional scale (not shown). Even though it is small, the LGM insolation forcing slightly counteracts the ice-sheet forcing during boreal winter and enhances it during boreal summer (figure 2a(ii)). The MH NH insolation forcing is negative from October to May and then positive. The asymmetry between boreal summer (approx. 18 W m^{-2}) and winter (approx. -10 W m^{-2}) maximum values results from the change in the length of the seasons [43]. The magnitude of nearly 20 W m^{-2} is similar to the one induced by the LGM ice-sheet (figure 2a).

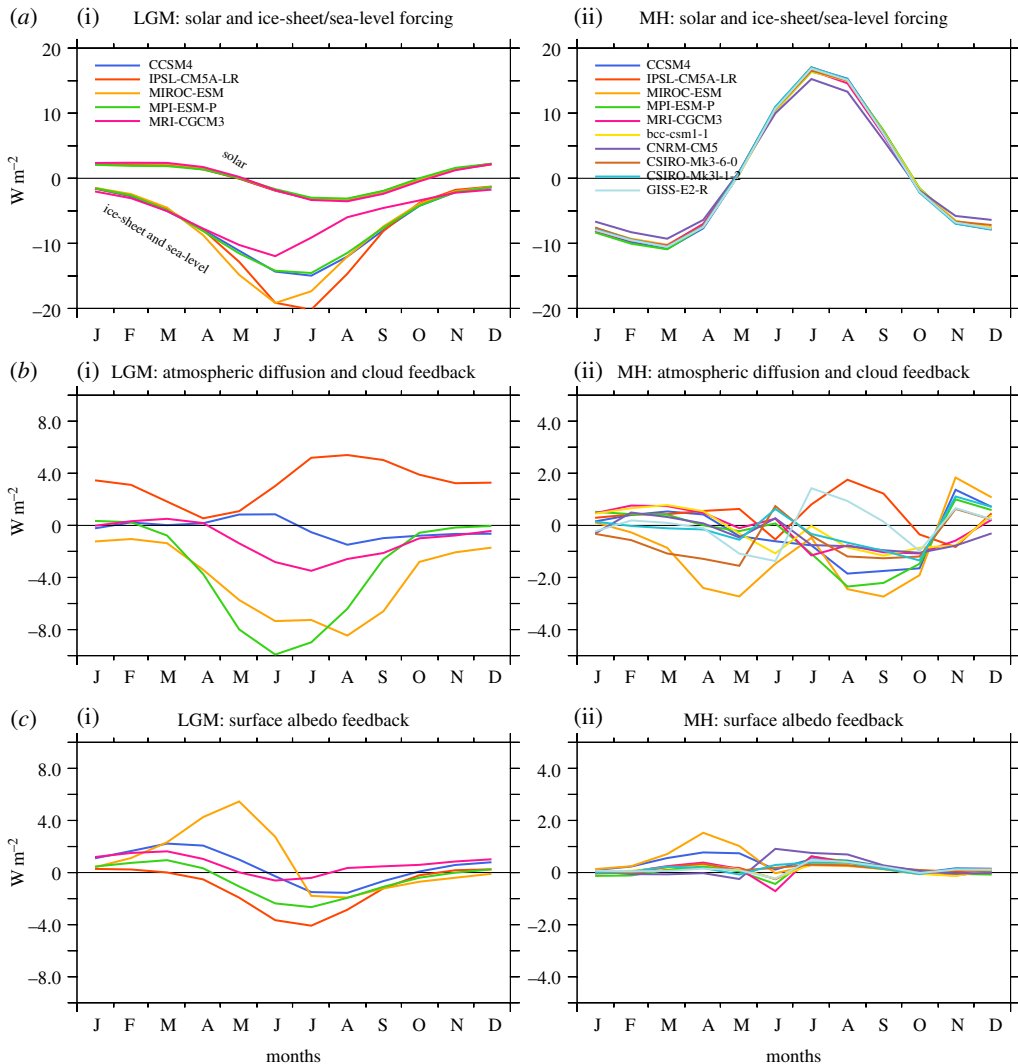


Figure 2. Shortwave radiative forcing (W m^{-2}) and feedbacks (W m^{-2}) averaged over the NH for the LGM (a(i), b(i), c(i)) and the MH (a(ii), b(ii), c(ii)). Each line corresponds to a particular model: (a) ice-sheet (only for the LGM) and insolation forcing; (b) atmospheric scattering (mainly from clouds) radiative feedback; and (c) surface albedo (from sea-ice snow and vegetation) radiative feedback. See text and references for details on the estimation of these feedbacks. (Online version in colour.)

The seasonal evolution of the SW cloud radiative feedback exhibits large differences from one model to the other (figure 2b(i)). Most models produce a negative feedback that counteracts the ice-sheet forcing and one model (IPSL-CM5A-LR) produces a positive feedback that enhances the ice-sheet forcing. The model spread is consistent with the LGM global annual mean SW cloud feedback parameter discussed in previous section. It follows the seasonal evolution of the ice-sheet forcing for only three of the models. The sign and the magnitude of the radiation change associated with this feedback are not correlated with the magnitude of ice-sheet forcing.

The SW cloud feedback in most models also tends to counteract the MH insolation forcing during boreal summer, except for IPSL-CM5A-LR and GISS-E2-R (figure 2b(ii)). Further investigation (not shown) reveals that in both cases the apparent mismatch of the IPSL model compared with the other models is due to mid-latitude cloud cover over the ocean, reinforcing the results from Vial *et al.* [40] for future climate sensitivity. Other models also show consistent differences with the model ensemble, such as MIROC-ESM, which shows a strong SW cloud

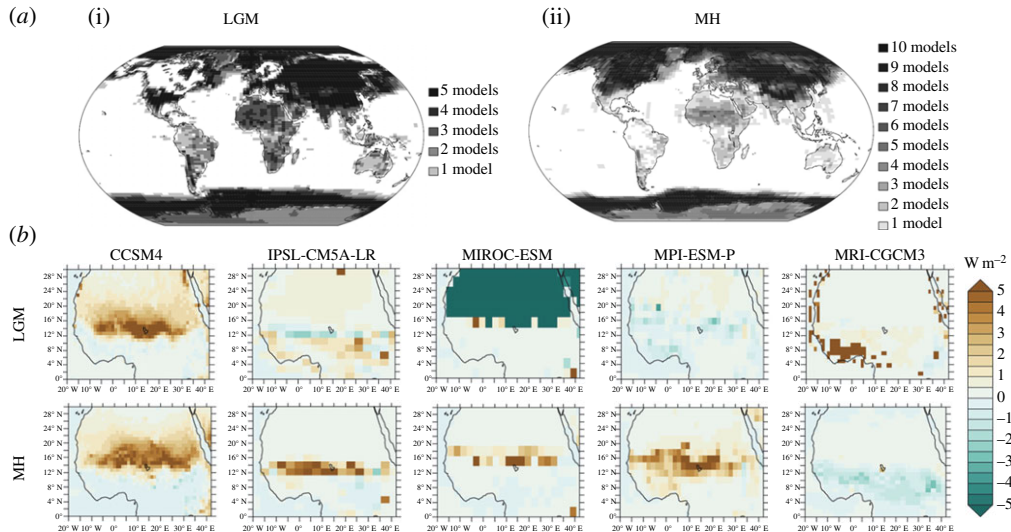


Figure 3. Land surface albedo radiative feedback. (a) Number of PMIP3 models producing an absolute albedo radiative feedback larger than 0.5 W m^{-2} for at least one month in the year at each grid point of the IPSL low-resolution grid were chosen as reference to interpolate all fields for the LGM (i) and the MH (ii). (b) Land surface albedo radiative feedback (W m^{-2}) in July–August–September resulting from vegetation changes for the five ESM models for which LGM and MH simulations and the needed variables are available in the PMIP3/CMIP5 database. (Online version in colour.)

feedback response. Comparison of the SW cloud feedback in different climates confirms that improving the representation of this feedback in climate models is a high priority. Future work should further improve our understanding on the different underlying processes operating, so as to find out which one is more important and should be fully evaluated to assess model credibility.

(b) Vegetation and snow feedbacks for LGM and MH

At the scale of the NH, the land surface albedo feedback is of smaller magnitude than the SW cloud feedback (figure 2c versus 2b). It reflects to first order the relative proportion of land and ocean. This feedback is restricted to sea-ice and snow covered areas, and for models with interactive vegetation to most continental regions (figure 3). The annual mean cycle of this feedback shares similarities between the two climates between January and August, with a tendency for a positive feedback in late boreal winter and spring and a negative one in boreal summer (figure 2c), limited to June in the case of the MH. This comparison also highlights that CCSM4 and MIROC-ESM have the strongest positive feedback from March to June in both climates. This corresponds to the period where sea-ice and snow increase most [13]. In the LGM, the period with negative feedback during summer reflects the reduction of sea-ice in the Arctic Ocean (figure 2c(i)). This counterintuitive result can be explained by the fact that the Arctic Ocean is actually much smaller at LGM compared with PI conditions, because of the extension of land or ice-sheets in this area. Even though sea-ice generally extends further south in the North Atlantic/Nordic Seas at the LGM, this does not compensate for the decrease from 70% to 42% of the area available for sea-ice formation north of 70° N . On the other hand, the negative feedback in June in the MH simulations is directly linked to a slight delay in the melting of sea-ice in response to the insolation forcing. At that time in the year the larger sea-ice and snow cover over land counteracts the warming induced by the larger insolation forcing. In summer the feedback becomes positive because of a larger sea-ice and snow melting (figure 2c(ii)). The different phasing and magnitude between the different curves in figure 2c highlight the different model responses and large uncertainties in high latitudes [44].

Figure 3 further highlights the regions where the different models show a consistent behaviour, considering five simulations for the LGM and 10 for the MH (table 1). All models except MRI-CGCM1 account for vegetation change at the LGM through LAI variations (CCSM4 and IPSL-CM5A-LR) or full dynamical vegetation (MIROC-ESM, MPI-ESM-P). CCSM4 also includes a representation of the nitrogen cycle [28]. Only five models account for vegetation change for the MH. Thereby this diagnostic can only reach a maximum of five models in continental regions that are not affected by snow cover changes. For this diagnostic, the surface albedo feedback computed for each model on its own grid was first interpolated on the coarser resolution IPSL-CM5A-LR grid. Then for each model a grid point is set to 1 if the absolute value of the surface albedo radiative feedbacks exceeds 0.5 W m^{-2} for at least one month. The threshold is chosen so that the radiative estimates are statistically significant at the grid point level. It results from the comparisons of the estimates obtained when using the PI and then the palaeoclimate as the climate reference, following what was done above for the global estimates at the LGM. The sum of the resulting 1/0 masks obtained for each model provides the numbers plotted in figure 3. They give an overview of model consistency. Regions with all models producing an albedo feedback correspond to sea-ice over the ocean and snow feedback over the continent. It affects both the NH and SH sea-ice and most of the Eurasian continent and North America (except where the LGM ice-sheet is located). In the tropics, these maps show very heterogeneous results both for the LGM and the MH, with one model producing vegetation changes almost everywhere. For the other models, the vegetation albedo feedback is more effective in the semi-arid regions, Sahara and, for the LGM, South America.

The albedo feedback of vegetation is further illustrated in figure 3 over West Africa for the five models for which LGM and MH simulations are available in the database, focusing on boreal summer during the African monsoon season. It reaches a few Watts per square metre and is thus less effective on the atmospheric circulation than the SW cloud radiative feedback that reaches $20\text{--}30 \text{ W m}^{-2}$ in this region. However, it has a local impact and locally reinforces or damps the African monsoon. These maps also show the lack of consistency between model results, even on the sign of the feedback for the LGM. This is similar to the large differences in precipitation changes simulated by the different models for this climate. As an example, CCSM4 shows a pronounced reduction of precipitation and a reduction of LAI at LGM compared with the PI. The larger surface albedo thus reflects more radiation back to space in the LGM than in the PI climate. The IPSL-CM5A-LR simulation shows a local enhancement of the African monsoon that is related to the fact that the thermohaline circulation is enhanced compared with the PI circulation, reinforcing the interhemispheric gradient in the tropical Atlantic and favouring the northward migration of the ITCZ over Africa and thereby the vegetation LAI. In this region the feedback is negative. In the other places over Africa, the drier climate contributes to the reduction of precipitation and of LAI, leading to a positive radiative feedback.

The response is more consistent for the MH (figure 3b). The vegetation albedo feedback is effective in the Sahel-Sahara region where it reaches up to 5 W m^{-2} . The exact location varies from one model to the other, so that the feedback on radiation and on precipitation is difficult to compare between those simulations. Part of the differences between models corresponds to differences in the precipitation change and the northward penetration of the monsoon flow onto the continent at the MH. As in PMIP2 simulations [45], this feedback is not sufficient and precipitation changes are still too small in the Sahel-Sahara compared with observations [6,46]. This analysis of the vegetation feedback for the two periods suggests that the representation of this feedback is still not satisfactory in climate models. Several factors could play a role. Some of them, such as the repartition of the different types of vegetation and of their associated characteristics, could have major impact. This has been shown to be a major factor in the representation of land-use in climate models [47] and therefore requires attention. Soil moisture has also been shown to drive the land-surface feedback in the Sahel [48] and is still poorly represented in this region. The intensity of the coupling between the land surface and the atmosphere is another important factor in West Africa where PMIP simulations show very

different intensities of evaporation depending on the convection and precipitation regimes [49]. Finally, model biases and the representation of the ITCZ are factors that precondition the surface humidity and vegetation growth. The MH precipitation differences with modern conditions are located to the north of the present-day ITCZ [50]. Model biases in the modern location of the ITCZ are therefore also a factor that partly impacts the MH vegetation feedback.

4. Model biases and vegetation feedback in Africa

The fact that land-surface albedo feedbacks are affected by model biases in the PI simulations makes it difficult to fully disentangle the part of the results that is purely because of model dynamical and physical representations of climate from the part that results from model tuning, initial state and implementation of the experimental protocol. To further illustrate this point we consider MH simulations run with two different versions of the IPSL climate model [33]: IPSL_CM5A_LR and IPSL_CM5B_LR. These two versions share the same ocean, sea-ice and land-surface models. The differences between them only arise from atmospheric physics and tuning [51]. Both versions use the same atmospheric deep convection scheme, but the IPSL_CM5B_LR version of the atmospheric component (LMDZ5B) includes a mass flux representation of the thermal plumes or rolls of the convective boundary layer, coupled to a bi-Gaussian statistical cloud scheme, as well as a parametrization of the cold pools generated below cumulonimbus by re-evaporation of convective precipitation [52]. These improvements in atmospheric physics lead to a better representation of the diurnal cycle of convection in the tropics [53], intraseasonal variability and ENSO dynamical and thermal feedbacks [33]. Despite these improvements the climatology of IPSL-CM5B-LR suffers from a large cold bias in the NH and warm bias in the SH and a poor representation of the ocean thermohaline circulation [33]. These climatological biases are not only the signature of the new physics but also of its interactions with the other model parametrizations, of the atmospheric model tuning that was necessary to obtain an equilibrated climate model without spurious long-term drift, and of the amplification of some of the biases by the coupling to the ocean, sea-ice and land-surface models.

The differences between the two IPSL model versions are illustrated for precipitation in figure 4. In the PI control simulations (figure 4a), the large-scale differences in temperature translate into a drier NH and a wetter SH in IPSL-CM5B-LR compared with IPSL-CM5A-LR. Over the tropical oceans, the ITCZ is shifted southward in IPSL-CM5B-LR, compared with IPSL-CM5A-LR, especially over the Atlantic and eastern Pacific. Over West Africa, IPSL-CM5B-LR is also slightly drier over the Sahel. Precipitation is more intense along the coast of the Gulf of Guinea, because of more intense convection there. In this region, the maximum ITCZ precipitation is larger and the northern flank of the ITCZ exhibits a sharper gradient towards the north. The ITCZ tends to be thinner with a larger amount of precipitation.

Both versions produce similar patterns of the MH change in precipitation over Africa, with a northward extension of the monsoon (figure 4b,c). This northward extension of monsoon rainfall into the Sahel-Sahara is, however, more pronounced in IPSL-CM5A-LR (figure 4c). In addition, the vegetation feedback is larger, reaching 5 W m^{-2} , whereas it is only of the order of 2 W m^{-2} and located further south in IPSL-CM5B-LR (figure 5). These differences in the vegetation feedback appear to be directly linked to differences in the representation of modern climatology. We do not pretend that differences in model physics have no impact on the simulated changes, but that biases in the temperature gradients and soil humidity have a larger impact. Indeed, two important factors enter into play here. Even though monsoon rainfall is almost similar in the two model versions in the PI simulations over land, the southward position of the ITCZ over the ocean in IPSL-CM5B-LR has an impact on the location of the MH precipitation change. The changes in precipitation are thus located further south in IPSL-CM5B-LR (figure 4b). This relationship between the modern location of the ITCZ and the location of precipitation changes was pointed out since the first phase of PMIP [50]. However, previous work suggests that this does not necessarily have an impact on the amount of precipitation change [46,54], because in some models deep precipitation regimes tend to be less efficient in the MH, so that the total

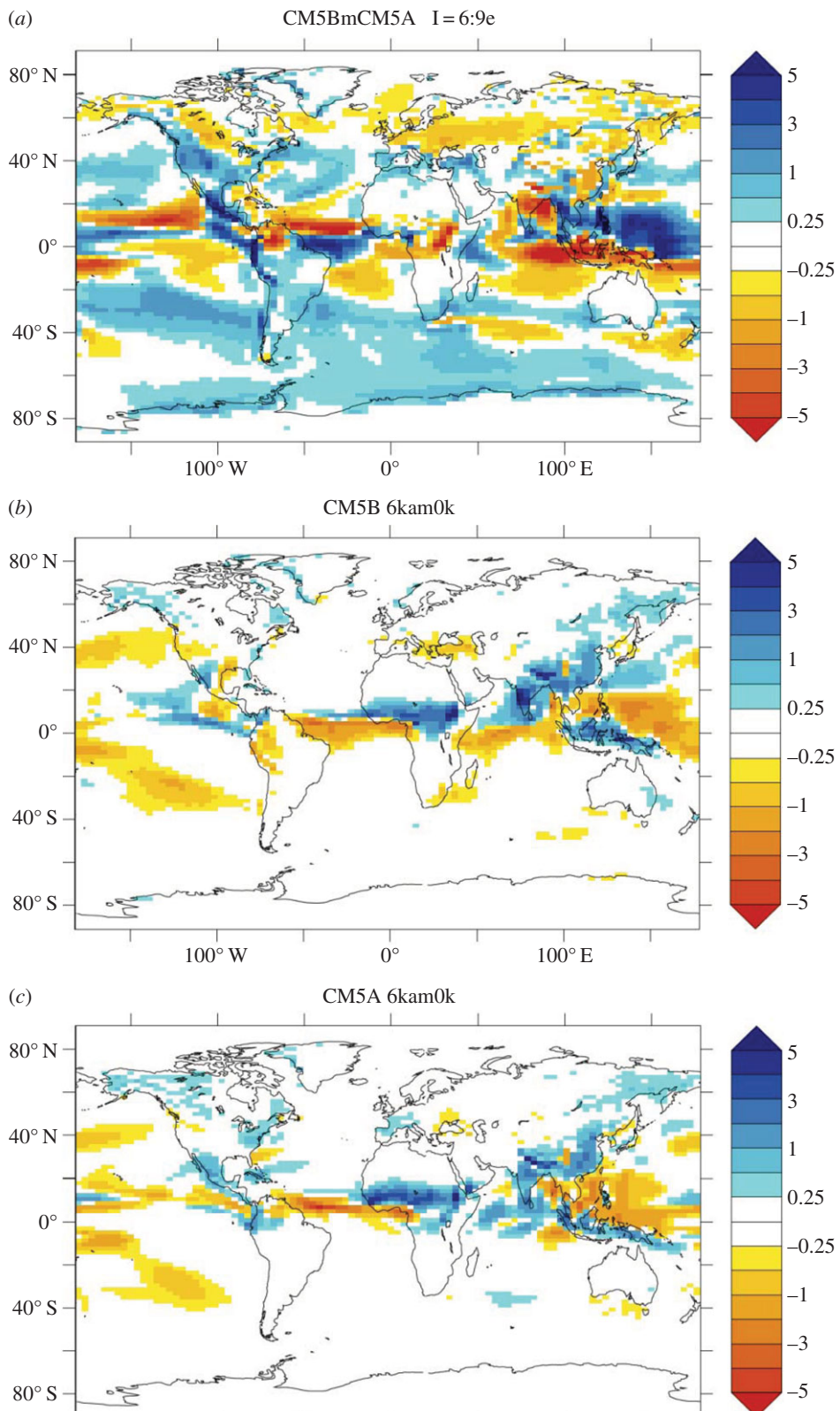


Figure 4. Comparison of IPSL-CM5B-LR and IPSL-CM5A LR precipitation (mm d^{-1}). (a) Differences between JJAS PI precipitation, (b) IPSL-CM5B-LR and (c) IPSL-CM5A-LR MH precipitation change (mm d^{-1}). (Online version in colour.)

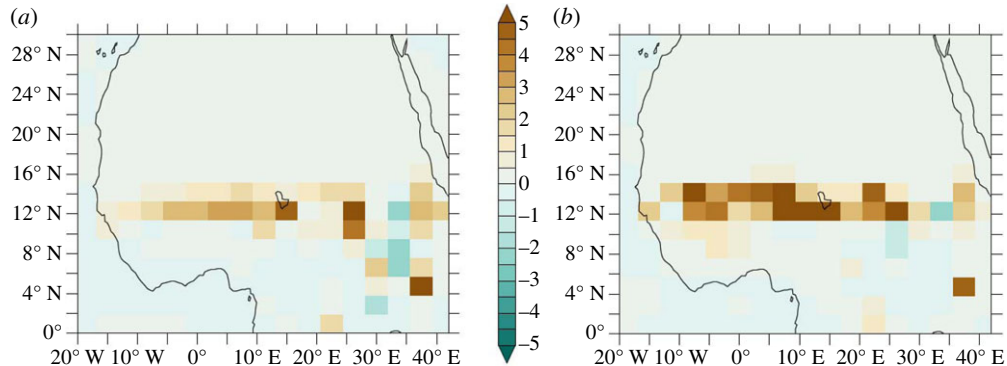


Figure 5. MH vegetation albedo radiative feedback (W m^{-2}) in the Afro-Asian monsoon region as simulated by (a) IPSL-CM5B-LR and (b) IPSL-CM5A-LR. (Online version in colour.)

change in precipitation results from the competition between this reduction of precipitation and the increase in frequency of deep convective regimes [49]. Also, the comparison of the two IPSL model versions shows that drier conditions in the Sahel region induces drier soils that prevent the development of vegetation and thereby limits local recycling and the northward inland penetration of the monsoon flow in IPSL-CM5B-LR. The changes in precipitation over the Sahel are thus smaller in IPSL-CM5B-LR than in IPSL-CM5A-LR, despite the fact that the new atmospheric physics tend to produce more intense precipitation in the continental ITCZ.

The differences in the location of the vegetation feedback in the different climate models and between the two versions of the IPSL model strongly suggest that the improvement of the representation of the ITCZ location in the PI control simulation is a prerequisite to properly trigger the vegetation feedback. Large-scale circulation and the interhemispheric contrast seem to be key factors. Local recycling and the coupling between the land surface and the atmospheric boundary layer is also an important factor in triggering precipitation [55]. This relationship and how it is represented in climate models also needs further attention before we can fully assess the role of the vegetation feedback in West Africa during the Holocene.

5. Conclusion

The comparison of the SW cloud and vegetation feedbacks across PMIP simulations for the LGM and the MH clearly shows that the SW cloud feedback is one of the major sources of uncertainty between model results. This factor was fully discussed by Yoshimori *et al.* [11] for the LGM, together with the fact that half of the models produce a negative feedback at the LGM, whereas it is a positive feedback for future climate [4,6]. Here we show that the different model properties for the LGM SW cloud feedback also hold for the MH when analysing the annual mean cycle of this feedback at the scale of the NH. In most models the SW cloud feedback counteracts the effect of the ice-sheet forcing at the LGM and of the insolation forcing at the MH. Two points need further investigation. First, the sign of the SW cloud radiative feedback for these two climates is opposite (except for the IPSL-CM5A-LR model) to the one it has for all these models for future climate. The question is therefore to determine if this is due to the nature of the forcing. Indeed for LGM ice-sheet and MH, the forcing is a shortwave forcing, whereas for future climate the forcing affects the LW radiation. This different forcing triggers different processes, which might be the reason for the difference in the sign of the SW cloud feedback between those two climates. The magnitude of the forcing (whatever its sign) remains quite similar between the LGM and future climate (see fig. 5.5 in [4]). This suggests that model differences in the magnitude and sign of the feedbacks provide a good fingerprint of model physics.

Because different climates are dominated by different types of forcings, acting in the SW or in the LW part of the radiative spectrum, the relative strength of the different feedbacks, and even the sign of some of them (like here for the SW) vary between climates. It explains why it

is difficult to find a direct relationship between past and future climate sensitivities. This does not mean that it is not possible to use past climate simulations to assess future climate sensitivity. It only implies that the road is more difficult than initially expected. Rather than looking for direct linkages it would be more appropriate to evaluate how the different models reproduce the reconstructed changes for different climates and what are the most important feedbacks involved. A solution would then be to isolate the past periods or the part of the year for which it is possible to assess a feedbacks acting as it does in climate projections. This was done, for example, by Masson-Delmotte *et al.* [56] in their comparison of past and future climates over Greenland and Antarctica. Similar feedbacks between the different periods develop during summer, when snow and sea-ice melt and the water vapour feedback becomes a dominant factor that amplifies the climate response.

A second aspect of the work presented here concerns the land-surface feedback. In several regions, the vegetation feedback is embedded in the snow feedback. For both the LGM and the MH, models consistently produce a large albedo feedback over sea-ice and most of the NH continent. Even though differences are found in the magnitude and seasonality of this feedback, model discrepancies are smaller for snow than for the vegetation feedback. Our illustration of the vegetation feedback over West Africa clearly shows the large heterogeneity of model results. LGM results show a large range, and reflect the heterogeneous results found for LGM precipitation changes over this region (not shown). Results are more consistent for the MH with a positive feedback over Sahel-Sahara for most models, but the exact location of the effect of vegetation varies a lot from one model to the other as does the pattern of precipitation changes. The comparison between two versions of the IPSL model also established that in this region the role of model physics in the simulated changes might be smaller than the direct effect of climatological biases in determining the location and magnitude of the vegetation albedo feedback. Biases in the model climatology resulting from the interactions between all model parametrizations, model tuning or large-scale biases, such as altered interhemispheric contrast, might be dominant. Soil moisture might also be determinant in triggering evapotranspiration and vegetation changes. The current generation of models does not perform better for this respect, and vegetation feedback is still a matter of concern. Another difficulty is that this feedback has only a regional or local impact. In addition to the surface albedo effect considered here, an estimate of the vegetation feedback on the evapotranspiration and thus on the atmospheric water content would be necessary. To go one step further one solution might be to estimate the realism of the effect of vegetation on evapotranspiration through convective regime sorted analyses following [49], so as to avoid to put too much emphasis on the geographical patterns that are not properly reproduced by climate models.

The simple method proposed here to estimate SW forcings and feedbacks is shown to be very efficient to highlight differences between periods and models. More complete analyses of the feedback estimates at model grid points offer additional information on the differences between models. As an example, the fact that the IPSL model produces different SW cloud feedback at the global or the hemispheric scales is mainly because of the mid-latitude ocean cloud cover. In other regions, the IPSL model results are more similar to those of the other models. Also, the results highlight the higher sensitivity of the MIROC-ESM and CCSM4 over snow and ice-covered area. This suggests that evaluation criteria need to be provided to assess if these simulations are correct or represent out-of-range results that should be dismissed from the PMIP model ensemble to produce the best estimate of the LGM or MH changes. Additional analyses should also consider LW forcings and feedbacks. This was outside the scope of this synthesis because a full partial radiative perturbation method using a radiative kernel would be required to do it. Also previous results suggest that model spread is smaller for water vapour and lapse rate or LW cloud feedback than it is for SW feedbacks [11]. Therefore, model improvement should focus on the reason for different SW cloud feedbacks between models and on the regional representation of vegetation and of its coupling with soil moisture and atmospheric boundary layer. Also comparing model results in different climate contexts allows to highlight systematic model behaviour. Future work will investigate how to use the available palaeoclimate reconstructions to determine which

radiative feedback response is more realistic. This is a way to define emerging constraints from palaeoclimate experiments that are relevant for the assessment of future climate projections.

Data accessibility. PMIP3 simulations are available on PMIP website <https://pmip3.lsce.ipsl.fr/>.

Authors' contributions. P.B. performed the feedback analyses and the writing of the manuscript. M.K. performed the LGM analyses, provided feedback on the whole manuscript and careful reading and corrections.

Competing interests. We declare we have no competing interests.

Funding. P.B. and M.K. were supported by the French National Research Agency under EL PASO grant (no. 2010 298 BLANC 60801). This project also serves the coordination and implementation of the PMIP3/CMIP5 simulations on ESGF database.

Acknowledgements. We acknowledge the World Climate Research Program's Working Group on Coupled Modelling, which is responsible for CMIP, and we thank the PMIP3 modelling groups for producing and making available their model output. The US Department of Energy's Program for Climate Model Diagnosis and Intercomparison provides coordinating support for CMIP, and led development of software infrastructure in partnership with the Global Organization for the Earth System Science Portals, the ESGF distributed database. We thank Jean-Yves Peterschmitt for his work on the PMIP database.

References

1. Joussaume S, Taylor KE. 1995 Status of the paleoclimate modeling intercomparison project. In *Proc. of the First International AMIP Scientific conf., WCRP-92*, Monterey, USA, pp. 425–430.
2. Braconnot P, Harrison SP, Kageyama M, Bartlein PJ, Masson-Delmotte V, Abe-Ouchi A, Otto-Bliesner B, Zhao Y. 2012 Evaluation of climate models using palaeoclimatic data. *Nat. Clim. Change* **2**, 417–424. ([doi:10.1038/nclimate1456](https://doi.org/10.1038/nclimate1456))
3. Schmidt GA *et al.* 2014 Using palaeo-climate comparisons to constrain future projections in CMIP5. *Clim. Past* **10**, 221–250. ([doi:10.5194/cp-10-221-2014](https://doi.org/10.5194/cp-10-221-2014))
4. Masson-Delmotte V *et al.* 2013 Information from paleoclimate archives. In *Climate Change 2013: The Physical Science Basis. Contribution of Working Group I to the Fifth Assessment Report of the Intergovernmental Panel on Climate Change* (eds TF Stocker, D Qin, G-K Plattner, M Tignor, SK Allen, J Boschung, A Nauels, Y Xia, V Bex, PM Midgley), pp. 383–464. Cambridge, UK: Cambridge University Press.
5. Harrison SP, Bartlein PJ, Brewer S, Prentice IC, Boyd M, Hessler I, Holmgren K, Izumi K, Willis K. 2014 Climate model benchmarking with glacial and mid-Holocene climates. *Clim. Dyn.* **43**, 671–688. ([doi:10.1007/s00382-013-1922-6](https://doi.org/10.1007/s00382-013-1922-6))
6. Flato G *et al.* 2013 Evaluation of climate models. In *Climate Change 2013: The Physical Science Basis. Contribution of Working Group I to the Fifth Assessment Report of the Intergovernmental Panel on Climate Change* (eds TF Stocker, D Qin, G-K Plattner, M Tignor, SK Allen, J Boschung, A Nauels, Y Xia, V Bex, PM Midgley), pp. 741–866. Cambridge, UK: Cambridge University Press.
7. Schmittner A, Urban NM, Shakun JD, Mahowald NM, Clark PU, Bartlein PJ, Mix AC, Rosell-Mele A. 2011 Climate sensitivity estimated from temperature reconstructions of the Last Glacial Maximum. *Science* **334**, 1385–1388. ([doi:10.1126/science.1203513](https://doi.org/10.1126/science.1203513))
8. Crucifix M. 2006 Does the Last Glacial Maximum constrain climate sensitivity? *Geophys. Res. Lett.* **33**, L18701. ([doi:10.1029/2006GL027137](https://doi.org/10.1029/2006GL027137))
9. Annan JD, Hargreaves JC. 2006 Using multiple observationally-based constraints to estimate climate sensitivity. *Geophys. Res. Lett.* **33**. ([doi:10.1029/2005gl025259](https://doi.org/10.1029/2005gl025259))
10. Schneider von Deimling T, Held H, Ganopolski A, Rahmstorf S. 2006 Climate sensitivity estimated from ensemble simulations of glacial climate. *Clim. Dyn.* **27**, 149–163. ([doi:10.1007/s00382-006-0126-8](https://doi.org/10.1007/s00382-006-0126-8))
11. Yoshimori M, Hargreaves JC, Annan JD, Yokohata T, Abe-Ouchi A. 2011 Dependency of feedbacks on forcing and climate state in physics parameter ensembles. *J. Clim.* **24**, 6440–6455. ([doi:10.1175/2011jcli3954.1](https://doi.org/10.1175/2011jcli3954.1))
12. Hargreaves JC, Annan JD, Ohgaito R, Paul A, Abe-Ouchi A. 2013 Skill and reliability of climate model ensembles at the Last Glacial Maximum and mid Holocene. *Clim. Past* **9**, 811–823. ([doi:10.5194/cp-9-811-2013](https://doi.org/10.5194/cp-9-811-2013))
13. Braconnot P *et al.* 2007 Results of PMIP2 coupled simulations of the Mid-Holocene and Last Glacial Maximum—part 2: feedbacks with emphasis on the location of the ITCZ and mid- and high latitudes heat budget. *Clim. Past* **3**, 279–296. ([doi:10.5194/cp-3-279-2007](https://doi.org/10.5194/cp-3-279-2007))

14. Bartlein PJ *et al.* 2011 Pollen-based continental climate reconstructions at 6 and 21 ka: a global synthesis. *Clim. Dyn.* **37**, 775–802. (doi:10.1007/s00382-010-0904-1)
15. Harrison SP, Bartlein PJ, Izumi K, Li G, Annan J, Hargreaves J, Braconnot P, Kageyama M. 2015 Evaluation of CMIP5 palaeo-simulations to improve climate projections. *Nat. Climate Change* **5**, 735–743. (doi:10.1038/Nclimate2649)
16. de Noblet-Ducoudre N, Claussen M, Prentice C. 2000 Mid-Holocene greening of the Sahara: first results of the GAIM 6000 year BP Experiment with two asynchronously coupled atmosphere/biome models. *Clim. Dyn.* **16**, 643–659. (doi:10.1007/s003820000074)
17. Ganopolski A, Kubatzki C, Claussen M, Brovkin V, Petoukhov V. 1998 The influence of vegetation-atmosphere-ocean interaction on climate during the Mid-Holocene. *Science* **280**, 1916–1919. (doi:10.1126/science.280.5371.1916)
18. Otto J, Raddatz T, Claussen M, Brovkin V, Gayler V. 2009 Separation of atmosphere-ocean-vegetation feedbacks and synergies for mid-Holocene climate. *Glob. Biogeochem. Cycles* **23**. (doi:10.1029/2009gl037482)
19. O’Ishi R, Abe-Ouchi A. 2009 Influence of dynamic vegetation on climate change arising from increasing CO₂. *Clim. Dyn.* **33**, 645–663. (doi:10.1007/s00382-009-0611-y)
20. Liu Z *et al.* 2007 Simulating the transient evolution and abrupt change of Northern Africa atmosphere-ocean-terrestrial ecosystem in the Holocene. *Quat. Sci. Rev.* **26**, 1818–1837. (doi:10.1016/j.quascirev.2007.03.002)
21. Wohlfahrt J, Harrison SP, Braconnot P, Hewitt CD, Kitoh A, Mikolajewicz U, Otto-Bliesner BL, Weber SL. 2008 Evaluation of coupled ocean-atmosphere simulations of the mid-Holocene using palaeovegetation data from the northern hemisphere extratropics. *Clim. Dyn.* **31**, 871–890. (doi:10.1007/s00382-008-0415-5)
22. Wang T, Wang H, Jiang D. 2010 Mid-Holocene East Asian summer climate as simulated by the PMIP2 models. *Palaeogeogr. Palaeoclimatol. Palaeoecol.* **288**, 93–102. (doi:10.1016/j.palaeo.2010.01.034)
23. Dallmeyer A, Claussen M, Otto J. 2010 Contribution of oceanic and vegetation feedbacks to Holocene climate change in monsoonal Asia. *Clim. Past* **6**, 195–218. (doi:10.5194/cp-6-195-2010)
24. Tian Z, Jiang D. 2013 Mid-Holocene ocean and vegetation feedbacks over East Asia. *Clim. Past* **9**, 2153–2171. (doi:10.5194/cp-9-2153-2013)
25. Kageyama M *et al.* 2013 Mid-Holocene and Last Glacial Maximum climate simulations with the IPSL model-part I: comparing IPSL_CM5A to IPSL_CM4. *Clim. Dyn.* **40**, 2447–2468. (doi:10.1007/s00382-012-1488-8)
26. Taylor KE, Stouffer RJ, Meehl GA. 2012 An overview of CMIP5 and the experiment design. *Bull. Am. Meteorol. Soc.* **93**, 485–498. (doi:10.1175/bams-d-11-00094.1)
27. Xin XG, Zhang L, Zhang J, Wu TW, Fang YJ. 2013 Climate change projections over East Asia with BCC_CSM1.1 climate model under RCP scenarios. *J. Meteorol. Soc. Jpn* **91**, 413–429. (doi:10.2151/jmsj.2013-401)
28. Gent PR *et al.* 2011 The community climate system model version 4. *J. Clim.* **24**, 4973–4991. (doi:10.1175/2011jcli4083.1)
29. Volodire A *et al.* 2013 The CNRM-CM5.1 global climate model: description and basic evaluation. *Clim. Dyn.* **40**, 2091–2121. (doi:10.1007/s00382-011-1259-y)
30. Rotstayn LD, Jeffrey SJ, Collier MA, Dravitzki SM, Hirst AC, Syktus JI, Wong KK. 2012 Aerosol- and greenhouse gas-induced changes in summer rainfall and circulation in the Australasian region: a study using single-forcing climate simulations. *Atmos. Chem. Phys.* **12**, 6377–6404. (doi:10.5194/acp-12-6377-2012)
31. Phipps SJ, Rotstayn LD, Gordon HB, Roberts JL, Hirst AC, Budd WF. 2011 The CSIRO Mk3L climate system model version 1.0-Part 1: description and evaluation. *Geosci. Model Dev.* **4**, 483–509. (doi:10.5194/gmd-4-483-2011)
32. Schmidt GA *et al.* 2006 Present-day atmospheric simulations using GISS ModelE: comparison to in situ, satellite, and reanalysis data. *J. Clim.* **19**, 153–192. (doi:10.1175/Jcli3612.1)
33. Dufresne JL *et al.* 2013 Climate change projections using the IPSL-CM5 Earth System Model: from CMIP3 to CMIP5. *Clim. Dyn.* **40**, 2123–2165. (doi:10.1007/s00382-012-1636-1)
34. Watanabe M, Chikira M, Imada Y, Kimoto M. 2011 Convective control of ENSO simulated in MIROC. *J. Clim.* **24**, 543–562. (doi:10.1175/2010jcli3878.1)
35. Jungclaus JH, Fischer N, Haak H, Lohmann K, Marotzke J, Matei D, Mikolajewicz U, Notz D, von Storch JS. 2013 Characteristics of the ocean simulations in the Max Planck Institute Ocean

- Model (MPIOM) the ocean component of the MPI-Earth system model. *J. Adv. Model. Earth Syst.* **5**, 422–446. (doi:10.1002/jame.20023)
36. Yukimoto S *et al.* 2012 A New Global Climate Model of the Meteorological Research Institute: MRI-CGCM3-model description and basic performance. *J. Meteorol. Soc. Jpn* **90A**, 23–64. (doi:10.2151/jmsj.2012-A02)
37. Taylor KE, Crucifix M, Braconnot P, Hewitt CD, Doutriaux C, Broccoli AJ, Mitchell JFB, Webb MJ. 2007 Estimating shortwave radiative forcing and response in climate models. *J. Clim.* **20**, 2530–2543. (doi:10.1175/Jcli4143.1)
38. Bony S *et al.* 2006 How well do we understand and evaluate climate change feedback processes? *J. Clim.* **19**, 3445–3482. (doi:10.1175/JCLI3819.1)
39. Hewitt CD, Mitchell JFB. 1996 GCM simulations of the climate of 6 kyr BP: mean changes and interdecadal variability. *J. Clim.* **9**, 3505–3529. (doi:10.1175/1520-0442(1996)009<3505:GSOTCO>2.0.CO;2)
40. Vial J, Dufresne JL, Bony S. 2013 On the interpretation of inter-model spread in CMIP5 climate sensitivity estimates. *Clim. Dyn.* **41**, 3339–3362. (doi:10.1007/s00382-013-1725-9)
41. Abe-Ouchi A *et al.* 2015 Ice-sheet configuration in the CMIP5/PMIP3 Last Glacial Maximum experiments. *Geosci. Model Dev. Discuss.* **8**, 4293–4336. (doi:10.5194/gmdd-8-4293-2015)
42. IPCC. 2013 *Climate Change 2013: The Physical Science Basis. Contribution of Working Group I to the Fifth Assessment Report of the Intergovernmental Panel on Climate Change*, p. 1535. Cambridge, UK: Cambridge University Press.
43. Joussaume S, Braconnot P. 1997 Sensitivity of paleoclimate simulation results to season definitions. *J. Geophys. Res.* **102**, 1943–1956. (doi:10.1029/96JD01989)
44. Berger M, Brandefelt J, Nilsson J. 2013 The sensitivity of the Arctic sea ice to orbitally induced insolation changes: a study of the mid-Holocene Paleoclimate Modelling Intercomparison Project 2 and 3 simulations. *Clim. Past* **9**, 969–982. (doi:10.5194/cp-9-969-2013)
45. Braconnot P *et al.* 2007 Results of PMIP2 coupled simulations of the Mid-Holocene and Last Glacial Maximum—part 1: experiments and large-scale features. *Clim. Past* **3**, 261–277. (doi:10.5194/cp-3-261-2007)
46. Perez-Sanz A, Li G, Gonzalez P, Harrison SP. 2014 Evaluation of seasonal climates of northern Africa and the Mediterranean in the CMIP5 simulations. *Clim. Past* **10**, 551–568. (doi:10.5194/cp-10-551-2014)
47. de Noblet-Ducoudre N *et al.* 2012 Determining robust impacts of land-use-induced land cover changes on surface climate over North America and Eurasia: results from the first set of LUCID experiments. *J. Clim.* **25**, 3261–3281. (doi:10.1175/jcli-d-11-00338.1)
48. Levis S, Bonan GB, Bonfils C. 2004 Soil feedback drives the mid-Holocene North African monsoon northward in fully coupled CCSM₂ simulations with a dynamic vegetation model. *Clim. Dyn.* **23**, 791–802. (doi:10.1007/s00382-004-0477-y)
49. Zheng WP, Braconnot P. 2013 Characterization of model spread in PMIP2 Mid-Holocene simulations of the African monsoon. *J. Clim.* **26**, 1192–1210. (doi:10.1175/jcli-d-12-00071.1)
50. Joussaume S *et al.* 1999 Monsoon changes for 6000 years ago: results of 18 simulations from the Paleoclimate Modeling Intercomparison Project (PMIP). *Geophys. Res. Lett.* **26**, 859–862. (doi:10.1029/1999gl900126)
51. Hourdin F *et al.* 2013 Impact of the LMDZ atmospheric grid configuration on the climate and sensitivity of the IPSL-CM5A coupled model. *Clim. Dyn.* **40**, 2167–2192. (doi:10.1007/s00382-012-1411-3)
52. Hourdin F *et al.* 2013 LMDZ5B: the atmospheric component of the IPSL climate model with revisited parameterizations for clouds and convection. *Clim. Dyn.* **40**, 2193–2222. (doi:10.1007/s00382-012-1343-y)
53. Rio C *et al.* 2013 Control of deep convection by sub-cloud lifting processes: the ALP closure in the LMDZ5B general circulation model. *Clim. Dyn.* **40**, 2271–2292. (doi:10.1007/s00382-012-1506-x)
54. Braconnot P, Loutre MF, Dong B, Joussaume S, Valdes P, Grps PP. 2002 How the simulated change in monsoon at 6 ka BP is related to the simulation of the modern climate: results from the Paleoclimate Modeling Intercomparison Project. *Clim. Dyn.* **19**, 107–121. (doi:10.1007/s00382-001-0217-5)
55. Koster RD *et al.* 2004 Regions of strong coupling between soil moisture and precipitation. *Science* **305**, 1138–1140. (doi:10.1126/science.1100217)
56. Masson-Delmotte V *et al.* 2011 Sensitivity of interglacial Greenland temperature and delta O-18: ice core data, orbital and increased CO₂ climate simulations. *Clim. Past* **7**, 1041–1059. (doi:10.5194/cp-7-1041-2011)